



CHORUS

This is the accepted manuscript made available via CHORUS. The article has been published as:

Anomalous bulk modulus in vanadate spinels

Z.-Y. Li, X. Li, J.-G. Cheng, L. G. Marshall, X.-Y. Li, A. M. dos Santos, W.-G. Yang, J. J. Wu, J.-F. Lin, G. Henkelman, T. Okada, Y. Uwatoko, H. B. Cao, H. D. Zhou, J. B. Goodenough, and J.-S. Zhou

Phys. Rev. B **94**, 165159 — Published 24 October 2016

DOI: [10.1103/PhysRevB.94.165159](https://doi.org/10.1103/PhysRevB.94.165159)

Anomalous bulk modulus in vanadate spinels

Z.-Y. Li¹, X. Li¹, J.-G. Cheng^{1,2,3}, L.G. Marshall¹, X.-Y. Li¹, A.M. dos Santos⁴, W.-G. Yang^{5,6}, J.J. Wu⁷, J.-F. Lin^{6,7}, G. Henkelman⁸, T. Okada³, Y. Uwatoko³, **H.B. Cao**⁴, H.D. Zhou⁹, J.B. Goodenough¹, J.-S. Zhou^{1*}

¹Materials Science and Engineering Program, University of Texas at Austin, Austin, Texas 78712, USA
²Beijing National Laboratory for Condensed Matter Physics and Institute of Physics, Chinese Academy of Sciences, Beijing 100190, China

³Institute for Solid State Physics, University of Tokyo, 5-1-5 Kashiwanoha, Chiba 277-8581, Japan

⁴Quantum Condensed Matter Division, Oak Ridge National Laboratory, Tennessee 37831, USA

⁵High Pressure Synergetic Consortium (HPSynC) and High Pressure Collaborative Access Team (HPCAT), Geophysical Laboratory, Carnegie Institute of Washington, Argonne, Illinois 60439, USA

⁶Center for High Pressure Science and Technology Advanced Research (HPSTAR), Shanghai 201900, China

⁷Department of Geological Sciences, Jackson School of Geosciences, University of Texas at Austin, Austin, Texas 78712 USA

⁸Department of Chemistry, University of Texas at Austin, Austin, Texas 78712 USA

⁹Department of Physics and Astronomy, University of Tennessee, Knoxville, Tennessee 37966, USA

All single-valent spinels are insulators. The relatively small activation energy in the temperature dependence of resistivity in vanadate spinels led to a speculation that the spinels are near the crossover from localized to itinerant electronic behavior and the crossover could be achieved under pressure. We have performed a number of experiments and calculations aimed at obtaining information regarding structural changes under high pressure for the whole series of vanadate spinels, as well as transport and magnetic properties under pressure for MgV₂O₄. We have also studied the crystal structure under pressure of wide-gap insulators ACr₂O₄ (**A= Mg, Mn, Fe, Zn**) for comparison. Moreover, the relationship between the bulk modulus and the cell volume of AV₂O₄ (**A=Mg, Mn, Fe, Co, Zn**) has been simulated by a DFT calculation. The proximity of AV₂O₄ spinels to the electronic state crossover under high pressure has been tested by three criteria (1) a predicted critical V-V bond length, (2) the observation of a sign change in the pressure dependence of Néel temperature, and (3) measurement of a reduced bulk modulus. The obtained results indicate that although the crossover from localized to itinerant π -bonding V-3d electrons in the AV₂O₄ spinels is approached by reducing under pressure the V-V separation R , the critical separation R_c is not reached by 20 GPa in CoV₂O₄ which has the smallest V-V separation in the AV₂O₄ (**A=Mg, Mn, Fe, Co, Zn**) spinels.

1. Introduction

Spinel oxides have long been the subject of geological research since they are naturally occurring minerals.¹⁻⁵ The spinel structure with AB_2O_4 formula consists of a network of edge-shared BO_6 octahedra with interstitial AO_4 tetrahedra. During World War II, physicists in France and Holland studied the collinear-spin ferromagnetic spinels in which antiferromagnetic spin-spin coupling between the tetrahedral and octahedral cations could be described by the Néel two-sublattice molecular-field model; description of non-collinear spin configuration caused by competitive antiferromagnetic B-B interactions was also developed by 1960.⁶ In recent years, interest in the physics community has returned to the problem of frustration caused by antiferromagnetic B-B interactions in the array of corner-shared tetrahedra where there is, in addition, an orbital degeneracy that introduces a complex orbital dynamics.⁷⁻¹⁸ In contrast to perovskite oxides in which a handful of single valent metallic oxides ranging from 3d to 5d transition metals (*e.g.* $SrVO_3$,¹⁹ $SrRuO_3$,²⁰ and ReO_3 ²¹) have been found, all single-valent spinel oxides are insulators. A perovskite AMO_3 consists of corner-shared octahedra and the electron bandwidth is determined by the M-O-M bond angle and the M-O bond length. In a spinel oxide AB_2O_4 , however, the electronic bandwidth is determined by the direct π -hybrid wavefunction overlap integral through the B-B bonds, which can be tuned by the chemical substitution at the A site. Although all single-valent spinels are insulators, the covalent contribution to the bonding is why integral valences implied from the charge ordering and orbital ordering patterns in the fully localized states have never been observed experimentally.⁷

The $A^{2+}V_2O_4$ spinels are Mott insulators; they have perhaps the smallest gap caused by electron-electron correlations in the single valent spinels. The V-V bond length in these spinels decreases as the A-site cation is replaced by cations in the order of $A = Cd, Mn, Fe, Mg, Zn, Co$.

Correspondingly, the activation energy for the hopping conduction also reduces progressively from $A = Cd$ to Co which is the smallest divalent cation in this series of spinels. A DFT calculation indicated that strong spin-orbit coupling is needed in order to justify the semiconductor state of the CoV_2O_4 .¹² Hydrostatic pressure is required to further reduce the V-V bond length in CoV_2O_4 . Interpretation of the transport property of CoV_2O_4 under pressure,¹⁶ however, is not straightforward. While there is an anomaly of the resistivity on cooling through a

magnetic transition temperature T_c in this ferrimagnet and a metallic-like resistivity is achieved under high pressure at $T < T_c$, the resistivity at $T < T_c$ is still too large for a metal and its temperature dependence at the lowest temperature remains activated to 8 GPa. Moreover, T_c increases with increasing pressure, which is a clear sign of a localized electronic state on the basis of the perturbation formula of the superexchange interaction. In order to clarify whether CoV_2O_4 is indeed at the crossover between localized electron and itinerant electronic behavior, it is critical to conduct a structural study under high pressure. For a phase at the crossover, its bulk modulus is normally lower than either in the metallic phase or in the insulator phase with the identical structure because of the coexistence of two equilibrium M-O bond lengths as, for example, in PbCrO_3 .^{22, 23} We report a comprehensive structural study on the entire series of AV_2O_4 spinels (A=Cd, Mn, Fe, Mg, Zn, Co) with *in-situ* high pressure X-ray and neutron diffraction at different temperatures. The behavior under high pressure is compared with that in another series of wide-band-gap spinels ACr_2O_4 .

2. Experimental Details

A detailed preparation of the AV_2O_4 sample preparation can be found in previous publications.²⁴ ²⁵ The ACr_2O_4 (A=Mg, Zn, Mn, Fe) polycrystalline samples were produced by conventional solid-state reaction. Stoichiometric mixtures of oxides AO (A=Mg, Zn, Mn, Fe; Alfa Aesar 99.99 %) and Cr_2O_3 (Alfa Aesar 99.9 %) were ground in an agate mortar with acetone and pressed into pellets. The pellets for A=Mg, Zn were heated in air at 1273 K for 24 h; the pellets for A=Mn, Fe were sealed in vacuum quartz tubes, which were then heated at 1273 K for 24 h. Similar annealing processes were repeated with intermediate grindings until phase-pure spinels as checked by XRD were achieved. High pressure conditions for the structural study were produced with symmetric diamond anvil cells (DACs) with 400 μm culet diamonds. A rhenium (Re) gasket was first pre-indented from 250 to ~ 50 μm in thickness, followed by drilling a hole of 190 μm diameter with an Electrical Discharge Machining system. Then, a sample pellet of ~ 50 μm wide and 25 μm thick formed by pressing the fine powder was loaded into the center of the drilled gasket hole and surrounded by several pieces of ruby spheres as the pressure calibrant. Hydrostaticity at the sample's place was ensured by loading neon gas by using a high-pressure gas loading system. The pressure range of this study went up to ~ 22 GPa. An initial pressure of about 0.4-0.7 GPa was maintained in the DACs after the gas loading. The *in-situ* high-pressure

and low-temperature XRD measurements were conducted with synchrotron radiation ($\lambda = 0.4136 \text{ \AA}$) at the Beamline 16-BM-D, HPCAT of the Advanced Photon Source, Argonne National Laboratory. The pressure at room temperature and low temperatures was controlled by a gear box and a helium-gas membrane, respectively, while an on-line ruby fluorescence system was used to monitor the pressure. The diffraction patterns were collected with a MAR345 image plate detector and were then converted into the format of intensity versus 2θ by using FIT2D software. The high-pressure structural study was also carried out at room temperature with a DAC mounted on a four-circle diffractometer (Bruker P4) with a Mo anode ($\lambda = 0.71 \text{ \AA}$). A small amount of CaF_2 powder was mixed with the sample to monitor the pressure inside the chamber, which was filled with a 4:1 methanol /ethanol mixture as the pressure medium. The structural information was extracted from Rietveld refinement of the obtained diffraction profiles with the FullProf program. **The powder sample of CoV_2O_4 sample used in this study was obtained by crushing a piece of single crystal. Single crystal neutron diffraction on a crystal CoV_2O_4 was performed at the HB-3A Four-circle Diffractometer at the High Flux Isotope Reactor(HFIR) at ORNL. Neutron wavelength of 1.005 \AA was used from a bent perfect Si-331 monochromator. 75 reflections were collected at 200 K and used for the structure refinement.** *In-situ* high pressure neutron diffraction measurements were measured at the SNAP beamline in the Spallation Neutron Source in ORNL. The SNAP instrument is a medium resolution time of flight diffractometer optimized for structural studies under high pressure. For this experiment, both detectors were placed at 90° relative to the incident beam and at 50 cm from the sample. The range of available incident neutron wavelengths was from 0.3 to 3.7 \AA . The sample was loaded in a Paris-Edinburgh press fitted with c-BN anvils. The encapsulating metal toroidal gaskets were fabricated with a null scattering TiZr alloy that does not add Bragg peaks to the powder data. The sample was loaded with a 4:1 methanol:ethanol mixture to act as a pressure medium. The cell was placed in a vertical orientation (allowing a view of the full detector 45° wide 2θ coverage). The cell was loaded inside a custom-made cryogenic system that allows the control of temperature between room temperature and 90 K. The combination of the wavelength bandwidth and the accessible angular range permitted the collection of data in a d-spacing range of 0.5 and 3.5 \AA . The measurements of resistivity under pressure were performed with a cubic anvil apparatus with *lava* as the gasket materials and glycerol as the pressure medium.²⁶

3. Results

3.1 CoV₂O₄

As reported by Kismarahardja *et al.*,¹⁶ the resistivity ρ of a CoV₂O₄ crystal decreases under pressure as shown in Fig.1. An even more dramatic pressure-induced change of ρ has been observed at a temperature below T_N , where a transition from $d\rho/dT < 0$ to $d\rho/dT > 0$ occurs. Therefore, it is interesting to study the pressure effect on the structure in both the paramagnetic phase and the magnetically ordered phase. We have performed XRD at 298 K $> T_N$ and 120 K $< T_N$. The cubic phase of CoV₂O₄ remains stable up to 22 GPa; see the fitting result for P=20 GPa as an example in Fig.2. The XRD patterns under different pressures at T=295 K and 120 K are displayed in Fig.3. The pressure dependence of cell volume at 295 K and 120 K in Fig.4 can be fit with the Birch-Murnaghan (BM) equation, which gives the bulk modulus $B_0=178(1)$ GPa for the paramagnetic phase at 295 K and a higher $B_0=199$ GPa at 120 K. This result indicates that, somewhat paradoxically, the ferrimagnetic phase is less compressible than that of the paramagnetic phase although a more dramatic pressure-induced change of the resistivity was observed at this temperature. It is also noticed that the error bar shown in Fig.4(a) is much larger in the fit at T=120 K than that at 295 K. Whereas T_N increases progressively under pressure, the resistivity at T $< T_N$ decreases more dramatically in the pressure range $0 < P < 6$ GPa in Fig.1. This observation motivates us to fit the V(P) data in two different pressure ranges, 0-6 GPa and 8-20 GPa in Fig.4(b). The new fittings indeed came with slightly smaller error bar size in the low pressure range; but it becomes even worse in the high pressure range. The new fittings suggest that the more conductive phase at 120 K and P > 6 GPa appear to have a much higher B_0 than that at lower pressure.

In the cubic spinel structure with the space group $Fd-3m$, the only atomic position for the refinement is a single atom coordination for the oxygen position (u,u,u). Since oxygen is shared by both the tetrahedral-site and the octahedral-site, an accurate determination of the u parameter under high pressure is necessary to find out the compressibility of tetrahedron and octahedron in the spinel. Unfortunately, the SXRd carries very little information about the oxygen position; the error bar of u from the refinement is too large to see any meaningful trend under pressure. To this end, **we turn to the neutron single crystal diffraction at ambient pressure and neutron powder**

diffraction under pressure. Neutron diffraction at cryogenic temperatures also provides information about magnetic structure and its evolution under high pressure.

The occupancies at Co-site and O-site are coupled to each other and one of them has to be fixed in the refinement. If we fixed the occupancy at O-site to 1, the occupancy at Co-site is over fully occupied and so we assumed the occupancy at Co-site is fully occupied and then refine the occupancies at V-site and O-site. Due to a tiny negative neutron scattering length at V site, the occupancy at V site cannot be determined accurately. All refined parameters are listed in Table.I.

By using neutron diffraction at SNAP, we have mapped out the crystal/magnetic structure of CoV_2O_4 in the temperature range of 90-300 K and the pressure range of 0-6.5 GPa. Typical diffraction patterns and their refinement results are displayed in Fig.5 and the structural parameters are shown in Table II. Since we have used the change of lattice parameter of CoV_2O_4 obtained from the SXRD as the pressure manometer in the neutron powder diffraction under high pressure, the bulk modulus cannot be checked independently. Fig.6 shows the pressure dependences of Co-O and V-O bond lengths and u parameter at different temperatures as well as the pressure dependences of magnetic moments on Co^{2+} and V^{3+} . Linear fitting on data points of V-O and Co-O at low pressures and at room temperature indicates that the Co-O bond is more compressible than the V-O bond, which is consistent with the general argument in insulators of spinel oxides, *i.e.* oxygen distances to trivalent cations are less compressible than those to divalent ones.²⁷ The refined value $u=0.239$ at ambient pressure is identical to that found **from single crystal neutron diffraction in Table I and** that in the literature.¹⁶ Based on the calculation of Madelung energy, a normal $\text{A}^{2+}(\text{B}^{3+})_2\text{O}_4$ spinel should have a $u \geq 0.2555$.⁵ Our refinement result suggests that the sample used in this study may be a partially inversed spinel, *i.e.* $(\text{Co}_{1-x}\text{V}_x)[\text{V}_{2-x}\text{Co}_x]\text{O}_4$. However, the structural refinement with a non-zero x gave an even poor result. This test indicates that the CoV_2O_4 sample is still a normal spinel.

The change of u parameter under pressure in Fig.6(c) is negligibly small and no clear trend can be discerned given the experimental uncertainty. An increase of u means that oxygen moves closer to the nearest tetrahedral cation in a $[111]$ direction, which reduces the volume of tetrahedra more quickly than that of octahedra under pressure. The observation of a smaller compressibility of the V-O bond than that of the Co-O bond observed would requires a monotonically increasing u under pressure. This contradiction suggests that the change in bond

length due to the pressure-induced reduction of the cell volume is more significant than the effect introduced by a small change of u parameter under pressure.

Neutron diffraction at 120 K and 90 K reveal the magnetic structure at different pressures. Fig.6(d) shows the refinement results of magnetic moment M at the Co^{2+} and V^{3+} sites. A $M=3.6 \mu_{\text{B}}$ at 90 K and ambient pressure is **considerably** higher than the expected value $3.0 \mu_{\text{B}}$ for Co^{2+} and the moment reported in the literature by neutron diffraction at 5 K.^{8,10} The moment at the Co^{2+} site reduces to a $M \leq 3.0 \mu_{\text{B}}$ under pressure. Reig-i-Plessis *et al.*⁸ reported recently a first order phase transition at 90 K in CoV_2O_4 spinel. The two-phase region at 90 K appears to influence our refinement with a single phase model. High pressure suppresses the phase transition by favoring the smaller volume phase at high temperature, therefore, the refinement at 90 K but under a pressure higher than ambient pressure gave a reasonable moment at Co^{2+} . This argument is further supported by the refinement results at 120 K. The refined moment stays below $3.0 \mu_{\text{B}}$ at all pressures at this temperature. The moment shows essentially no change under pressure within the measurement uncertainty, which means that the localized picture for electrons at the Co^{2+} site is not altered under pressure up to 6 GPa. A significantly reduced moment $\sim 0.7 \mu_{\text{B}}$ at V^{3+} which is consistent with the reported value,^{8,10} was treated as a sign for delocalized electrons.⁸ However, a reduced moment ($\sim 0.65 \mu_{\text{B}}$) at V^{3+} has been found in other spinels AV_2O_4 ($\text{A}=\text{Cd}, \text{Mg}, \text{Zn}$) in which CdV_2O_4 has the longest V-V bond length in the family of vanadate spinels, which makes this argument questionable. On the other hand, Maitra and Valenti¹³ have shown that the unquenched orbital momentum is antiferromagnetically coupled to the spin, so as to reduce the net total moment below $1 \mu_{\text{B}}$. Thus, a slight increase of the moment at V^{3+} under pressure in Fig.5(d) may reflect a reduction of the orbital moment, which means that wavefunctions for electrons at V^{3+} become more extended under pressure.²⁸

3.2 MgV_2O_4

Simply from the consideration of V-V bond length, the electron bandwidth of MgV_2O_4 is close to that in CoV_2O_4 . Both spinels have much smaller activation energies in the transport properties than that in CdV_2O_4 and MnV_2O_4 .¹⁶ Based on the compressibility of the V-V bond length from the structural study for CoV_2O_4 above, the critical V-V bond length where a transition from $dp/dT < 0$ to $dp/dT > 0$ occurs can be induced in MgV_2O_4 under a pressure $P < 10$ GPa. We have measured the resistivity to 8 GPa in Fig.7(a) with a cubic multianvil apparatus. Whereas the

resistivity decreases with pressure over the entire temperature range, no obvious anomalies are revealed. It was not possible for us to monitor the resistivity change to temperatures below T_N since the magnitude of resistance is higher than the input resistance of the voltmeter used in the measurement. We have measured the pressure dependence of magnetic transitions of MgV_2O_4 by using a piston-cylinder device up to 8 GPa. Unfortunately, due to the combination of a weak moment on V^{3+} and the contribution from the high pressure cell, the magnetization does not show a clear sign at the cubic to tetragonal transition at T_{N1} and the subsequent magnetic transition at T_{N2} .²⁹ However, dM/dT illustrated in Fig.7(b) reveals anomalies corresponding to these transitions. Both transition temperatures decrease linearly with increasing pressure, as shown in Fig.7(c). These results together with those reported earlier³⁰ for CdV_2O_4 and ZnV_2O_4 complete the pressure dependence of structure/magnetic transitions in the vanadate spinels with non-magnetic A-site cations. The obvious change in the pressure dependence of T_N for the three vanadates is a transition from $dT_N/dP > 0$ to $dT_N/dP < 0$ as the V-V bond length decreases from CdV_2O_4 to MgV_2O_4 and ZnV_2O_4 as shown in Fig.7(d).

3.3 Bulk modulus of AV_2O_4 and ACr_2O_4

The bulk modulus B_0 of the paramagnetic phase of CoV_2O_4 is similar to that of most perovskite oxides and spinel oxides. In order to extract the influence of the electronic state on the bulk modulus, the bulk modulus of all vanadate spinels AV_2O_4 is obtained systematically and B_0 is studied as a function of the V-V bond length. Fig.8 shows the pressure dependence of the cell volume of AV_2O_4 and results of fitting $V(P)$ to a BM equation. All curves except $A=Co$ were obtained with a DAC mounted on a diffractometer with Mo anode radiation. All bulk modulus B_0 obtained by fitting $V(P)$ to a BM equation are plotted in Fig.9; B_0 decreases monotonically as the cell volume reduces from $A=Cd$ to Fe. The trend of decreasing B_0 reaches its minimum at $A=Fe$. The relatively higher values of B_0 found for $A=Co$, Zn, and Mg do not appear to be correlated to the unit cell volume; the relative change among these three spinels can be justified by number of d electrons as demonstrated in the following paragraph. For comparison, we have also measured the bulk modulus of chromate spinels ACr_2O_4 which are wide band-gap insulators; these results are also displayed in Fig.9.

3.4 Simulation of the bulk modulus of AV_2O_4 spinels by first-principles calculations.

Density functional theory calculations were performed to simulate the structure and bulk modulus of AV_2O_4 ($A = \text{Cd, Mn, Fe, Mg, Zn}$ and Co) spinels using the Vienna Ab initio Simulation Package.³¹⁻³³ Core electrons were described within the projector augmented wave framework³⁴. Valence electrons were expanded in a plane wave basis with an energy cut-off of 600 eV. Electronic exchange and correlation was described with the PBEsol+U functional.³⁵ In our calculations on-site Coulomb and exchange terms were applied at the metal ions to prevent delocalization of the d-electrons, caused by artificial self-interaction of electrons in the DFT approach. Values of $U = 4.25$ eV and $J_H = 1.58$ eV were applied to the V ions; values for the other A-site cations are listed in Table III. In our calculations, the geometry of all atoms were relaxed until the residual force dropped below 2.5 meV/\AA .

For each vanadate spinel, the ground state energy (E) versus the cell volume (V) was calculated by incrementally changing the lattice constant of the material. Figure 10, as an example, shows the E vs V curve for CoV_2O_4 . The bulk modulus B_0 , was obtained by fitting the $E(V)$ curve to the Murnaghan equation with the procedure described in the reference³⁶. The calculated values of B_0 versus equilibrium cell volume are superimposed in Fig. 9. Interestingly, ZnV_2O_4 is calculated to have the smallest volume rather than CoV_2O_4 which has been found to have the smallest volume experimentally. There are two obvious differences between calculated results and experimental results: (1) our calculated B_0 values are found to increase along the series $A=\text{Cd}$ to Fe , and (2) the trend that B_0 increases for spinels with a smaller cell volume continues for $A= \text{Co}$ and Zn . This qualitative difference is discussed in the following section. The unusual cell volume dependence in the three spinels $A=\text{Mg, Co, and Zn}$ found experimentally are, however, nicely reproduced by the DFT calculations. The total number of d electrons of the A-cation appears to play a significant role in determining B_0 for these spinels; the d electron occupation of d^0 (Mg^{2+}), d^7 (Co^{2+}) and d^{10} (Zn^{2+}) correlate with the bulk moduli, $B_0=175$ GPa (Mg), 191.2 GPa(Co), and 192.5 (Zn). We should note that the calculated B_0 values are larger than experiment for all members in the AV_2O_4 family. Even larger calculated values of B_0 for AV_2O_4 have been reported recently.³⁷ Although the same procedure³⁶ was used to calculate B_0 , the authors obtained the $E(V)$ curve by using the local density approximation (LDA) functional. It is well known that LDA underestimates the lattice constant and will result in a much larger B_0 . On the other hand, the generalized gradient approximation (GGA)³⁸ tends to overestimate lattice constants. In our calculations, we used the PBEsol functional which takes a linear combination of

GGA and LDA to optimize properties of solids such as the lattice constant, which is why our calculated values are closer to the experimental data than that reported by Lal and Pandey.³⁷

4. Discussion

Briefly comparing the phase diagrams of the spinels AV_2O_4 and the perovskites $RNiO_3$ provides a useful guide for the present research; the phase diagrams of these two oxide family are displayed in Fig.11. The control parameter for the electronic bandwidth is the V-V separation R in spinels whereas it is the rare earth ionic radius (IR) which tunes the Ni-O-Ni bond angle and Ni-O bond length in perovskites. In $RNiO_3$, the orbital overlap integral t , *i.e.* the bandwidth, is proportional to the IR. Therefore an increase of T_N as the IR increases (up to 1.16 Å) is consistent with the perturbation expression of the superexchange interaction $T_N \sim J \propto t^2/U$, where U is the on-site correlation energy. The T_N versus IR is truncated by the phase boundary of a first-order metal-insulator transition. T_N is completely suppressed in the rhombohedral phase where the metallic phase is stabilized to the lowest temperature. A high-pressure structural study carried out at room temperature showed a clear minimum of the bulk modulus near $IR = r(Nd_{0.5} + Sm_{0.5})$ where the first order transition phase boundary crosses room temperature; the minimum B_0 at $Nd_{0.5}Sm_{0.5}NiO_3$ can be interpreted by a coexistence of two equilibrium bond lengths in the phase at the crossover. In contrast, for AV_2O_4 spinels, the experimental data do not fall on a monotonic curve in the plot of T_N versus $1/R$. Instead, they can be separated into two groups, one with magnetic cations $A = Mn, Fe, Co$ and the other with non-magnetic cations $A = Cd, Mg, Zn$. The superexchange interaction between two magnetic sublattices in the former appears to enhance the Néel temperature of the ferrimagnetic phase. The superexchange formula is fulfilled in both groups, *i.e.* T_N increasing as $1/R$ increases. In particular, a dramatic increase of T_N in CoV_2O_4 resembles a higher T_N of $SmNiO_3$ which is near the phase boundary of first-order phase transition. The high-pressure structural study in this work has verified that the V-V bond separation R in both the paramagnetic phase and the magnetic phase is significantly shorter than the critical value (will be discussed below) at $P = 8$ GPa at which the resistivity shows more dramatic change in the magnetically ordered phase than that in the paramagnetic phase. A continuous increase of T_N under high pressure from the resistivity measurement¹⁶ can be mapped out in the plot of T_N versus $1/R$. The $1/R$ dependence of T_N changes at the R value corresponding to CoV_2O_4 . The dramatic increase of T_N from $A=Fe$ to $A=Co$ seems to be related to the change of exchange interaction between A and V in addition to the shortening of the V-V bond length.

Whether the AV_2O_4 spinels are at the crossover or approaching the crossover can be further examined along three lines of evidence.

I. The critical V-V separation R_c .

Motivated by the formation of V-V dimmers in VO_2 and trimmers in $LiVO_2$,³⁹⁻⁴¹ the AV_2O_4 spinels was studied in the 1960s to determine there would be a universal critical V-V separation R_c for V clustering across shared octahedral-site edges on approaching a Mott transition from the localized–electron side. Based on the bond length dependence of the activation energy E_a derived from the resistivity measurements, Rogers *et al.* have postulated a critical V-V separation $R_c \sim 2.97 \text{ \AA}$.⁴² The V-V separation R can be directly calculated through the formula $R = V^{1/3} \sqrt{2}/4$ and it is indicated on the right vertical axis of Fig.8. The plot makes it clear that most of AV_2O_4 spinels would have $R < R_c$ under modest pressure. This critical bond length appears to be too large. Here are examples, (a) R_c is reached around $P > 1 \text{ GPa}$ in MgV_2O_4 ; however, it remains an insulator up to 8 GPa as shown in Fig. 7; (b) The R_c is crossed at $P=4.4 \text{ GPa}$ for FeV_2O_4 ; but the $\rho(T)$ is still activated in both paramagnetic and ferrimagnetic phases up to 8 GPa.¹⁶ The situation in CoV_2O_4 is a bit complicated. At $P= 6 \text{ GPa}$ (corresponding to $R=2.94 \text{ \AA}$) while the resistivity in the paramagnetic phase is still activated, a $d\rho/dT > 0$ was observed in the ferrimagnetic phase below T_N . However, according to the compressibility data at $T=120 \text{ K}$, the transition from $d\rho/dT < 0$ to $d\rho/dT > 0$ is not accompanied by a softening lattice expected for the phase at crossover. From all these observations, a much smaller R_c than 2.97 \AA , perhaps a value well below 2.88 \AA (corresponding to 20 GPa) is expected to trigger a insulator-metal transition in AV_2O_4 .

II. Changing the sign of dT_N/dP .

To have a complete solution of the Mott-Hubbard Hamiltonian remains challenging. A numerical solution by Rozenberg *et al.* illustrated the evolution of T_N as a function of U ; T_N peaks at crossover.⁴³ The diagram of the localized to itinerant electron transition can be easily converted into an experimentally testable version, *i.e.* $dT_N/dP > 0$ for localized electrons and $dT_N/dP < 0$ for itinerant electrons given that the bandwidth increases under pressure. From this criteria, the spinels AV_2O_4 ($A = \text{Mn},^{30} \text{Fe},^{16} \text{Co}^{16}$) showing a $dT_N/dP > 0$ should have localized d electrons. Based on this criteria, the transition from $dT_N/dP > 0$ in CdV_2O_4 to $dT_N/dP < 0$ in ZnV_2O_4 and MgV_2O_4 in Fig.7(d) would indicate that the crossover is approached in these spinels. While a $dT_N/dP < 0$ was found in MgV_2O_4 , the resistivity in Fig.7(a) clearly does not support the

assertion that an itinerant electronic state is approached in this spinel. The criteria for identifying whether the crossover is approached fails here because the magnetic transition is close to the cubic to tetragonal structural change and the magnetic transition may be associated with a small volume change. The volume change on crossing the transition may make pressure favor the phase at $T < T_N$ for $A = \text{Cd}$ and the phase at $T > T_N$ for $A = \text{Zn}$ and Mg .

III. Anomalous bulk modulus.

As demonstrated in RNiO_3 , B_0 reduces for the phase at the crossover relative to either the localized electron phase or the itinerant electron phase. In order to distinguish whether the change of electron state indeed plays a role behind the complicated behavior of B_0 versus $1/V_0$ found for AV_2O_4 in Fig. 9, we turn to the Anderson-Nafe (AN) rule,⁴⁴ *i.e.* $B_0 V_0 = \text{constant}$. The rule which can be derived starting from an interatomic potential in ionic bonds, has been found to be universal for insulators.⁴⁵ Results from the DFT calculations for AV_2O_4 shown as a dashed line in Fig. 9 follow essentially the AN rule. Predicting a localized to itinerant electron transition relies on subtle differences in energy which are difficult to capture by using standard DFT methods. This transition will also be sensitive to the choice of the on-site Coulomb interaction U ; our choice of U for each AV_2O_4 spinel results in an insulating ground state, which is why the AN rule works well. It is also clear that the experimental results for a wide gap spinel family ACr_2O_4 roughly follow the AN rules. Therefore, the dramatic difference between the calculated results and experimental finding for AV_2O_4 reflects a significantly softening lattice as the V-V bond length decreases, which implies that AV_2O_4 are not at but approaching the crossover. Gradual reductions of the magnetic moment at Co site and the orbital momentum at V site in CoV_2O_4 under pressure determined by neutron diffraction under pressure support this argument.

5. Conclusion.

The vanadate spinel oxides show a progressive reduction of the activation energy derived from the resistivity as the V-V separation R reduces and a critical $R_c = 2.97 \text{ \AA}$ has been predicted based on the behavior of activation energy versus R . In-situ high-pressure structural studies verified that the predicted R_c can be achieved under pressure to 8 GPa in several members of the spinel family. On crossing the predicted R_c , the responding changes of physical properties are totally different between members in the family. The activation energy shows very little change in FeV_2O_4 , MgV_2O_4 ; but it indeed vanishes within a narrow temperature range in the ferrimagnetic

phase of CoV_2O_4 . However, a finite activation energy remains in the paramagnetic phase up to 8 GPa. These results indicate a $R_c = 2.97 \text{ \AA}$ is not a true critical V-V separation for the localized to itinerant electron transition. A sign change from $dT_N/dP > 0$ to $dT_N/dP < 0$ found in CdV_2O_4 , ZnV_2O_4 , and MgV_2O_4 has also been proven to be irrelevant to the transition. The systematic measurements of the bulk modulus in the whole family reveal an important relationship between B_0 and the cell volume and therefore the V-V bond length. A clear deviation from the prediction based on the Anderson-Nafe rule indicates unambiguously that the electronic state of AV_2O_4 approaches the crossover as the V-V separation decreases. However, the transition to a metallic phase may occur at even higher pressures, at least 20 GPa where the V-V separation is less than 2.88 \AA in the AV_2O_4 .

Acknowledgments

JSZ and JBG were supported by the NSF-DMR-1122603 and the Welch Foundation (F-1066). JGC was supported by the National Basic Research Program of China (Grants No. 2014CB921500), the National Science Foundation of China (Grants No. 11304371, 11574377). HDZ thanks the support from NSF-DMR-1350002. The research at Oak Ridge National Laboratory was supported by the U.S. Department of Energy, Office of Science, Scientific User Facilities Division (ADSG). Support for the calculations was provided by the Welch Foundation (F-1841) and the Texas Advanced Computing Center.

*jszhou@mail.utexas.edu

Table I The structure parameters of CoV_2O_4 measured at 200K by single crystal neutron diffraction at HB-3A at HFIR.

| atom | type | site | x | y | z | $U_{\text{equiv}}(\text{\AA}^2)$ | occupancy |
|------|------|------|-------------|-------------|-------------|----------------------------------|-----------|
| Co1 | Co | 8b | 3/8 | 3/8 | 3/8 | 0.3(1) | 1 |
| V1 | V | 16c | 0 | 0 | 0 | 0.3 | 1.2(2) |
| O1 | O | 32e | 0.23941(26) | 0.23941(26) | 0.23941(26) | 0.6(1) | 0.996(36) |

The space group is Fd-3m , $a=8.407(10) \text{ \AA}$. $R_f=0.0494$. $\chi^2=0.52$.

Table II Results of Rietveld refinement of neutron powder diffraction for CoV_2O_4 .

| | ambient | 1.76GPa | 2.98GPa | 5.17GPa | 5.48GPa | 6.35GPa |
|-----------------|-----------|-----------|-----------|-----------|-----------|-----------|
| a | 8.4070(2) | 8.3842(3) | 8.3665(3) | 8.3358(4) | 8.3316(4) | 8.3198(5) |
| μ | 0.2393(1) | 0.2398(1) | 0.2398(1) | 0.2396(2) | 0.2395(2) | 0.2401(2) |
| R_{wp} | 1.84 | 1.45 | 1.48 | 1.48 | 1.59 | 1.79 |
| χ^2 | 2.17 | 1.42 | 1.39 | 1.06 | 1.50 | 0.83 |

Space group $Fd-3m$ (No. 227), Co (0.375, 0.375, 0.375), V (0, 0, 0), O (μ , μ , μ)

Table II (continue) Magnetic moment on Co and V at low temperatures under different pressures

| | ambient | 1.76GPa | 2.98GPa | 5.17GPa | 5.48GPa | 6.35GPa |
|------------|---------|---------|---------|---------|---------|---------|
| M(Co)_90K | 3.61(9) | 2.8(1) | 2.7(1) | 2.8(1) | 2.7(1) | 2.4(1) |
| M(Co)_120K | 2.8(1) | 2.3(1) | 2.6(1) | 2.5(1) | 2.7(1) | 2.3(1) |
| M(V)_90K | 0.7 (1) | 0.7(1) | 1.1(1) | 1.1(2) | 1.1(2) | 1.0 (2) |
| M(V)_120K | 0.5 (1) | 0.6(1) | 1.0(1) | 1.2(2) | 1.0 (2) | 0.8(2) |

Table III On-site Coulomb (U) and exchange (J) parameters of A-site cations used in the DFT calculations.

| A-site atom | Cd^{2+} | Mn^{2+} | Fe^{2+} | Mg^{2+} | Zn^{2+} | Co^{2+} |
|-------------|------------------|------------------|------------------|------------------|------------------|------------------|
| U / eV | 2.5 | 4.5 | 5.5 | 0.0 | 0.0 / 0.0 | 4.3 |
| J / eV | 0.5 | 0.7 | 0.5 | 0.0 | 0.0 / 0.0 | 1.0 |

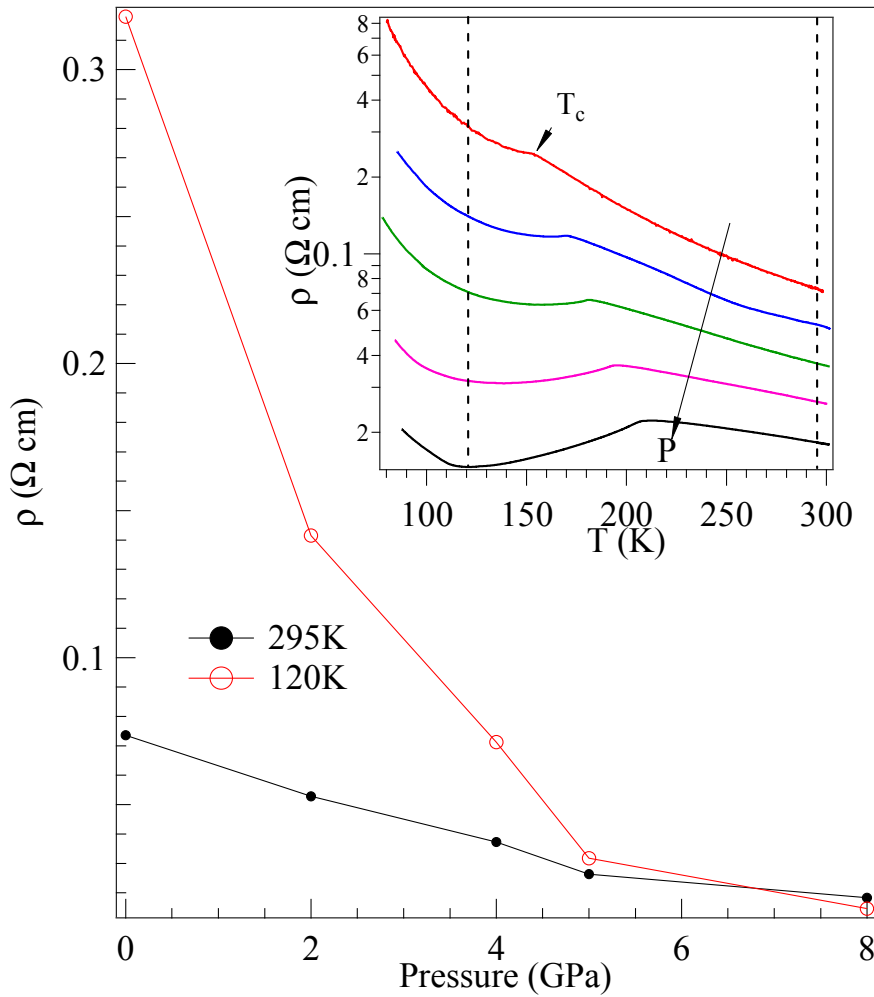


Fig.1 (Color online) The pressure dependence of resistivity of CoV_2O_4 at different temperatures. The inset: temperature dependence of resistivity at different pressures, dashed lines shows the temperatures where we have performed the structural study under pressure. The data are after ref.16.

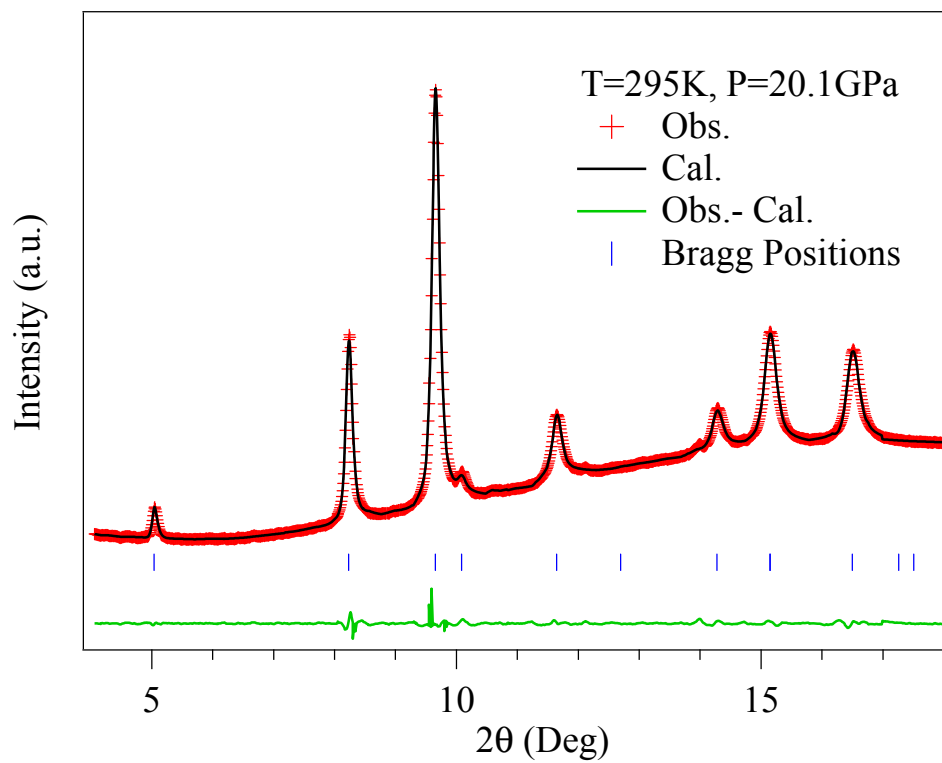


Fig.2 (Color online) An X-ray diffraction pattern of CoV_2O_4 with synchrotron radiation and the result of the Rietveld refinements.

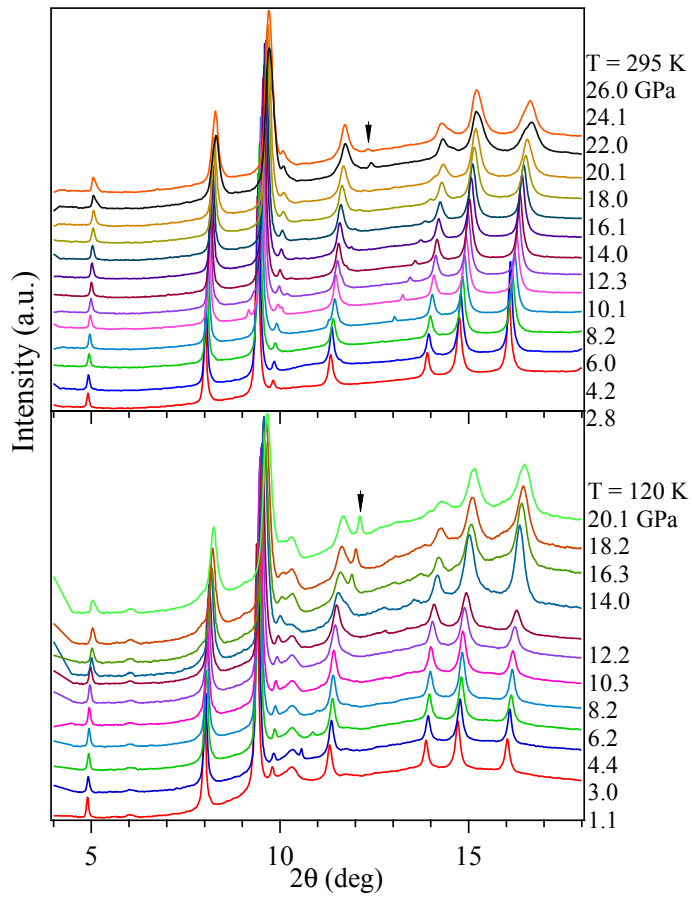


Fig.3 (Color online) X-ray diffraction patterns of CoV_2O_4 with synchrotron radiation under different pressures at 295K (top) and 120 K (bottom). The peak at $2\theta \sim 12^\circ$ indicated by an arrow is from the cubic phase of neon consolidated under high pressure.

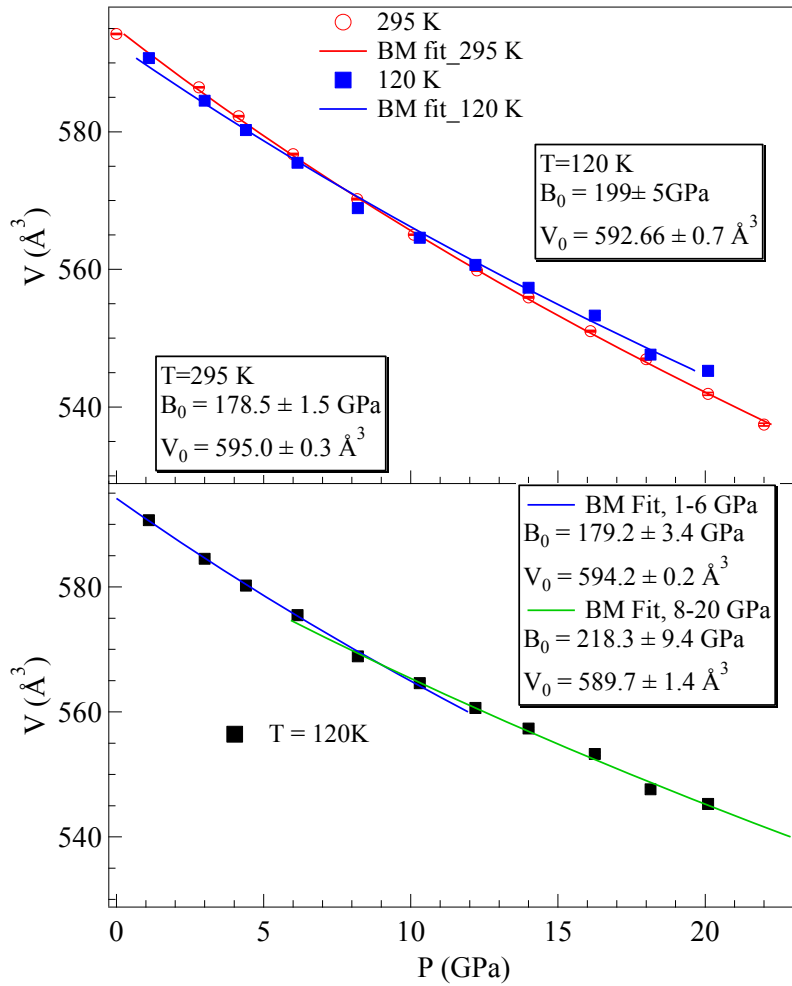


Fig.4 (a) (Color online) The pressure dependence of cell volume and the fitting results to the Birch-Murnaghan equation at 295 K and 120 K; (b) $V(P)$ curve at 120 K and the fitting results at two separate pressure ranges $0 < P < 6$ and $8 < P < 20$ GPa.

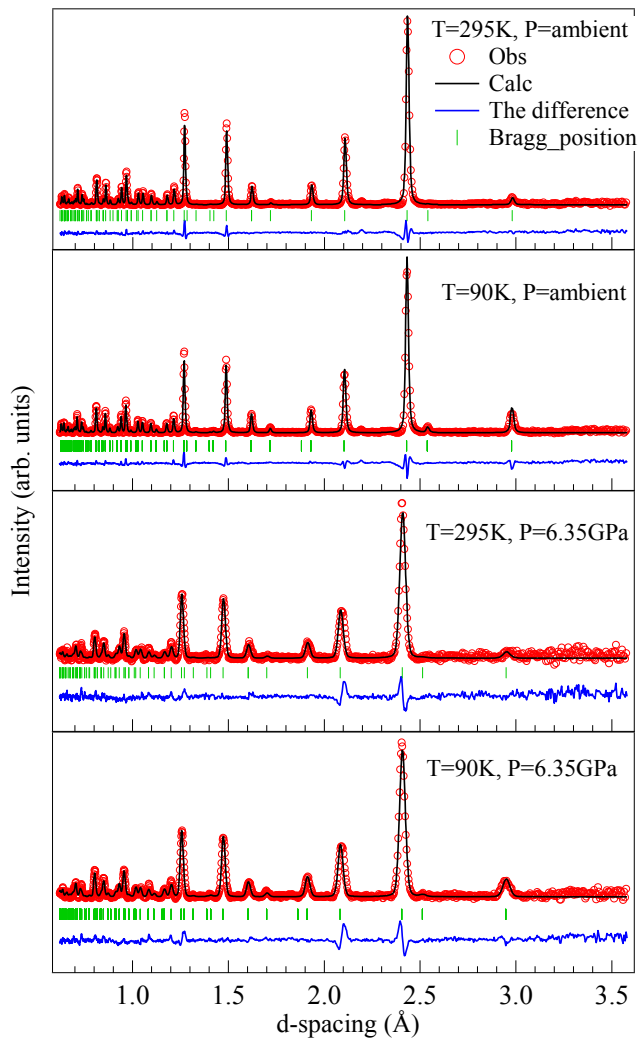


Fig.5 (Color online) Examples of neutron diffraction of CoV_2O_4 at different pressures and temperatures and the results of the Rietveld refinements.

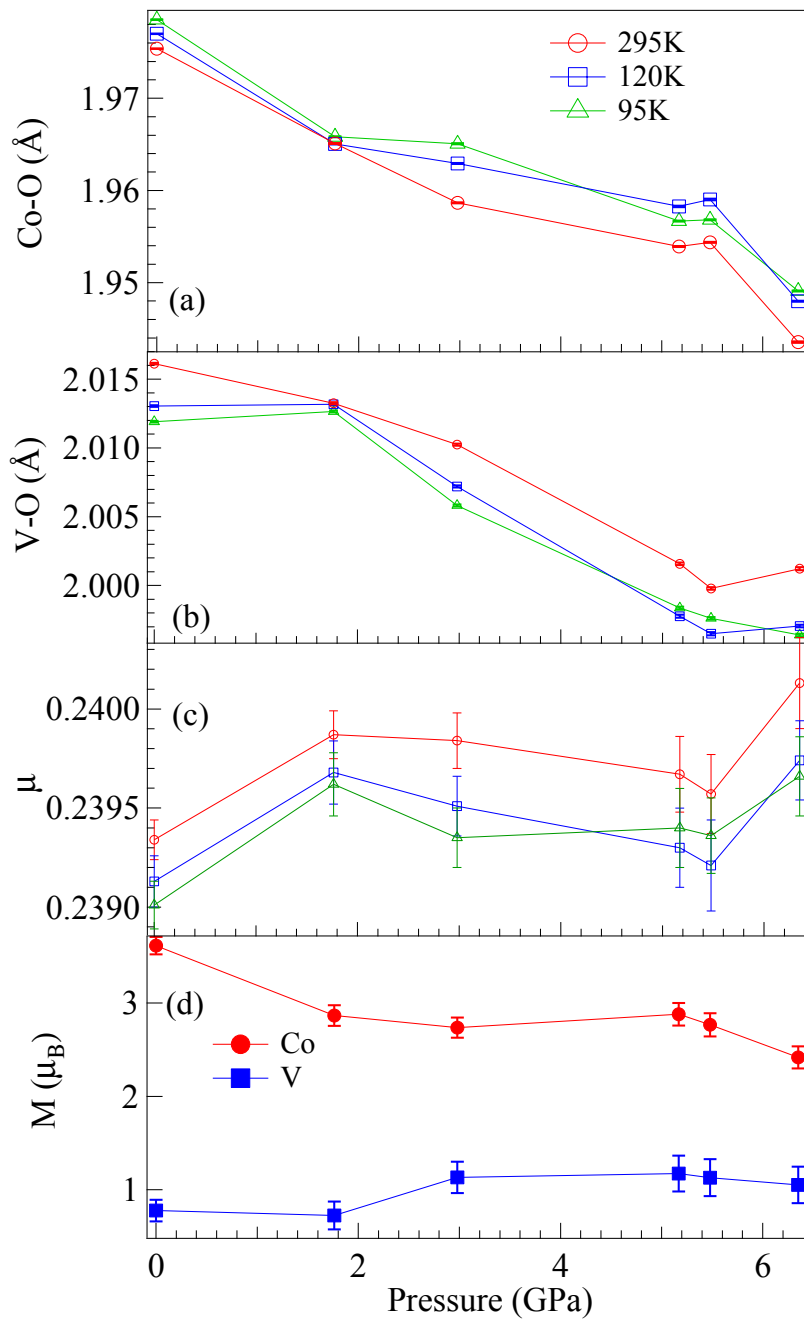


Fig.6 (Color online) Pressure dependences of cation-oxygen bond lengths, the u parameter for the oxygen position, and the magnetic moments on cations of CoV_2O_4 .

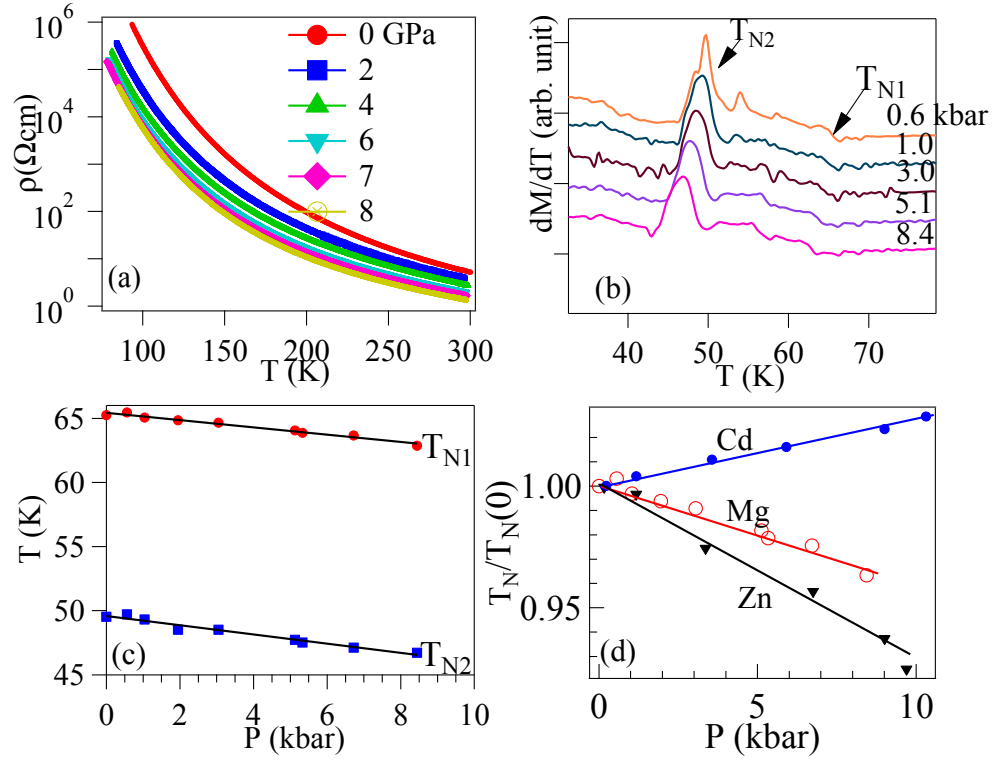


Fig.7 (a) (Color online) The temperature dependence of resistivity of MgV_2O_4 under different pressures, (b) the temperature dependence of derivative of the magnetization, (c) pressure dependences of two magnetic transition temperature, (d) the pressure dependences of the normalized T_N for AV_2O_4 ($A=Cd, Mg, Zn$). The data of CdV_2O_4 and ZnV_2O_4 are after ref.29.

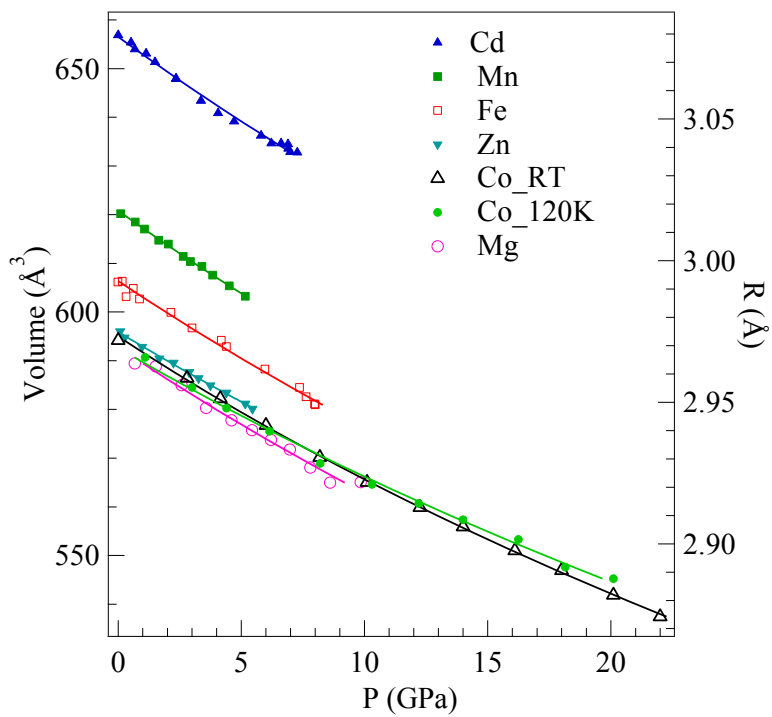


Fig.8 (Color online) The pressure dependence of cell volume of AV_2O_4 ($A=Cd, Mn, Fe, Zn, Co, Mg$); the vertical axis on the right denotes the V-V separation in the spinels.

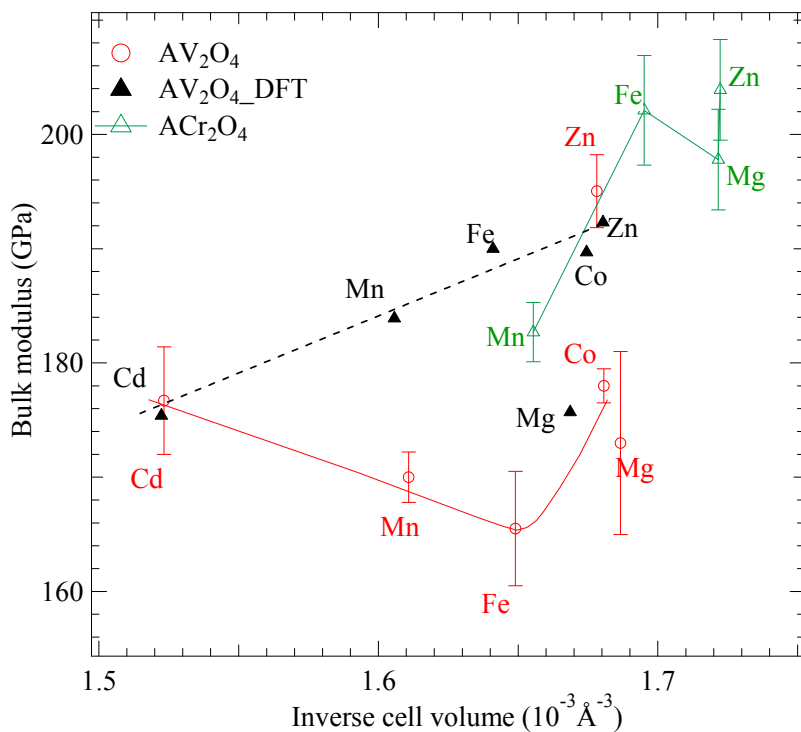


Fig.9 (Color online) The bulk modulus versus the inverse cell volume of AV_2O_4 ($A=Cd, Mn, Fe, Zn, Co, Mg$) and ACr_2O_4 ($A=Mn, Fe, Zn, Mg$) and the DFT results of AV_2O_4 .

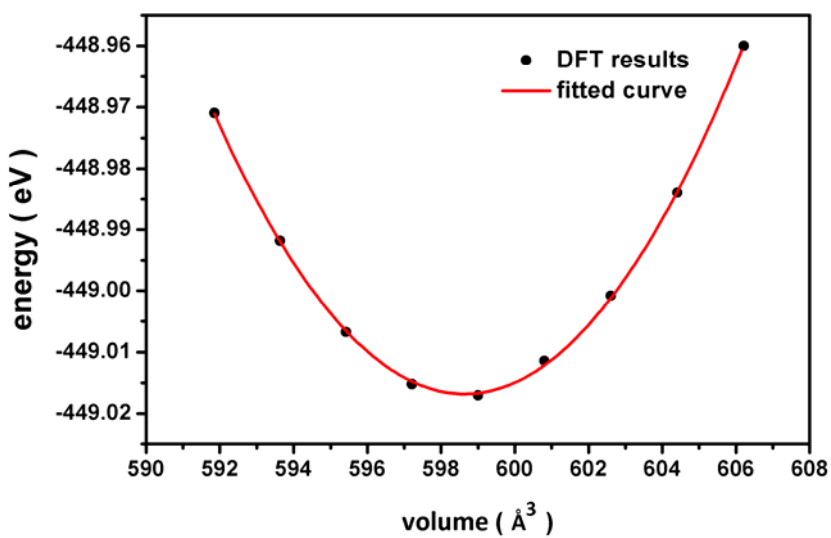


Fig.10 (Color online) The ground state energy versus cell volume and the fitting result to the Murnaghan equation for CoV_2O_4 .

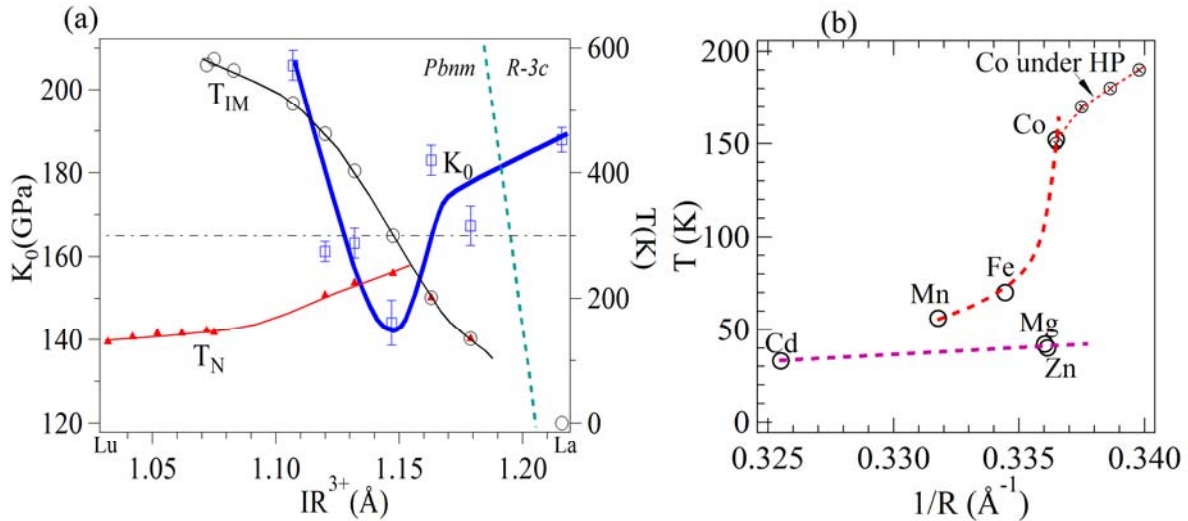


Fig.11 (Color online) Phase diagrams of perovskites RNiO_3 (R =rare earth) and spinels AV_2O_4 .

- 1 H. S. C. O'Heill and A. Navrotsky, *Ameri. Minera.* **68**, 184 (1983).
- 2 R. M. Hazen, *Science* **259**, 206 (1993).
- 3 L. W. Finger, R. M. Hazen, and A. M. Hofmeister, *Phys. Chem. Minerals* **13**, 215 (1986).
- 4 R. M. Hazen and L. W. Finger, *J. Geophys. Res.* **84** (1979).
- 5 R. J. Hill, J. R. Craig, and G. V. Gibbs, *Phys. Chem. Minerals* **4**, 317 (1979).
- 6 J. B. Goodenough, *Magnetism and the Chemical Bond* (Interscience Publishers, New York, 1963).
- 7 P. G. Radaelli, *New J. Phys.* **7**, 53 (2005).
- 8 D. Reig-i-Plessis, D. Casavant, V. O. Garlea, A. A. Aczel, M. Feyngenson, J. Neuefeind, H. D. Zhou, S. E. Nagler, and G. J. MacDougall, *Phys. Rev. B* **93**, 014437 (2016).
- 9 G. J. MacDougall, I. Brodsky, A. A. Aczel, V. O. Garlea, G. E. Granroth, A. D. Christianson, T. Hong, H. D. Zhou, and S. E. Nagler, *Phys. Rev. B* **89**, 224404 (2014).
- 10 R. Koborinai, S. E. Dissanayake, M. Reehuis, M. Matsuda, T. Kajita, H. Kuwahara, S. H. Lee, and T. Katsufuji, *Phys. Rev. Lett.* **116**, 037201 (2016).
- 11 V. Pardo, S. Blanco-Canosa, F. Rivadulla, D. I. Khomskii, D. Baldomir, H. Wu, and J. Rivas, *Phys. Rev. Lett.* **101**, 256403 (2008).
- 12 R. Kaur, T. Maitra, and T. Nautiyal, *J. Phys. Condens. Matter* **26**, 045505 (2014).
- 13 T. Maitra and R. Valenti, *Phys. Rev. Lett.* **99**, 126401 (2007).

14 O. Tchernyshyov, Phys. Rev. Lett. **93**, 157206 (2004).
15 S. H. Lee, et al., Phys. Rev. Lett. **93**, 156407 (2004).
16 A. Kismarahardja, J. S. Brooks, A. Kiswandhi, K. Matsubayashi, R. Yamanaka, Y.
Uwatoko, J. Whalen, T. Siegrist, and H. D. Zhou, Phys. Rev. Lett. **106** (2011).
17 Y. Kato, G.-W. Chern, K. A. Al-Hassanieh, N. B. Perkins, and C. D. Batista, Phys. Rev.
Lett. **108**, 247215 (108).
18 S. H. Lee, et al., J. Phys. Soc. Japan **79**, 011004 (2010).
19 R. Eguchi, et al., Phys. Rev. Lett. **96**, 076402 (2006).
20 G. Cao, S. MacCall, M. Shepard, J. E. Crow, and R. P. Guertin, Phys. Rev. B **56**, 321
(1997).
21 T. P. Pearsall and C. A. Lee, Phys. Rev. B **10**, 2190 (1974).
22 W. Xiao, D. Tan, X. Xiong, J. Liu, and J. Xu, PANS **107** (2010).
23 J.-G. Cheng, et al., PNAS **112**, 1670 (2015).
24 A. Kiswandhi, J. Ma, J. S. Brooks, and H. D. Zhou, Phys. Rev. B **90**, 155132 (2014).
25 R. Sinclair, J. Ma, H. B. Cao, T. Hong, M. Matsuda, Z. L. Dun, and H. D. Zhou, Phys.
Rev. B **92**, 134410 (2015).
26 N. Mori, H. Takahashi, and N. Takeshita, High Pressure Research **24**, 225 (2004).
27 J. M. Recio, R. Franco, A. M. Pendas, M. A. Blanco, L. Pueyo, and R. Pandey, Phys.
Rev. B **63**, 184101 (2001).
28 J. B. Goodenough, Phys. Rev. **171**, 466 (1968).
29 H. Mamiya, M. Onoda, T. Furubayashi, J. Tang, and I. Nakatani, J. Appl. Phys. **81**, 5289
(1997).
30 S. Blanco-Canosa, F. Rivadulla, V. Pardo, D. Baldomir, J.-S. Zhou, M. Garcia-
Hernandez, M. A. Lopez-Quintela, J. Rivas, and J. B. Goodenough, Phys. Rev. Lett. **99**,
187201 (2007).
31 G. Kresse and J. Furthmuller, Computational Materials Science **6** (1996).
32 G. Kresse and J. Furthmuller, Phys. Rev. B **54**, 11169 (1996).
33 G. Kresse and J. Hafner, Phys. Rev. B **47** (1993).
34 P. E. Blochl, Phys. Rev. B **50**, 17953 (1994).
35 J. P. Perdew, A. Ruzsinszky, G. I. Csonka, O. A. Vydrov, G. E. Scuseria, L. A.
Constantin, X. Zhou, and K. Burke, Phys. Rev. Lett. **102**, 039902 (2009).
36 <http://gilgamesh.cheme.cmu.edu/doc/software/jacapo/appendices/appendix-eos.html>.
37 S. Lal and S. K. Pandey, arXiv:1605.04152v1 (2016).
38 J. P. Perdew, K. Burke, and M. Ernzerhof, Phys. Rev. Lett. **78**, 3865 (1996).
39 J. B. Goodenough, Phys. Rev. **117** (1960).
40 T. A. Hewston and B. L. Chamberland, J. Phys. Chem. Solids **48**, 97 (1987).
41 J. B. Goodenough, Phys. Rev. **120**, 67 (1960).
42 D. B. Rogers, R. J. Amott, A. Wold, and J. B. Goodenough, J. Phys. Chem. Solids **347-**
360, 347 (1963).
43 M. J. Rozenberg, G. Kotliar, and X. Y. Zhang, Phys. Rev. B **49**, 10181 (1994).
44 O. L. Anderson and J. E. Nafe, J. Geophys. Res. **72**, 5754 (1967).
45 D. L. Anderson and O. L. Anderson, J. Geophys. Res. **75**, 3494 (1970).